

# Mechanisms of Atlantic Meridional Overturning Circulation (AMOC) Variability in a Coupled Ocean–Atmosphere GCM

Boyin HUANG<sup>\*1</sup>, ZHU Jiang<sup>2</sup>, and YANG Haijun<sup>2</sup>

<sup>1</sup>National Climatic Data Center, NOAA, Asheville, NC 28801, USA

<sup>2</sup>Laboratory for Climate and Ocean–Atmosphere Studies, and Department of Atmospheric and Oceanic Sciences, School of Physics, Peking University, Beijing 100871

(Received 24 January 2013; revised 1 May 2013; accepted 14 May 2013)

## ABSTRACT

The mechanisms involved in the variability of Atlantic Meridional Overturning Circulation (AMOC) are studied using a 2000-yr control simulation of the coupled Fast Ocean–Atmosphere Model (FOAM). This study identifies a coupled mode between SST and surface heat flux in the North Atlantic at the decadal timescale, as well as a forcing mode of surface heat flux at the interannual timescale. The coupled mode is regulated by AMOC through meridional heat transport. The increase in surface heating in the North Atlantic weakens the AMOC approximately 10 yr later, and the weakened AMOC in turn decreases SST and sea surface salinity. The decreased SST results in an increase in surface heating in the North Atlantic, thus forming a positive feedback loop. Meanwhile, the weakened AMOC weakens northward heat transport and therefore lowers subsurface temperature approximately 19 yr later, which prevents the AMOC from weakening. In the forcing mode, the surface heat flux leads AMOC by approximately 4 yr.

**Key words:** Atlantic Meridional Overturning Circulation, AMOC variability, coupled mode, and forcing mode

**Citation:** Huang, B. Y., J. Zhu, and H. J. Yang, 2014: Mechanisms of Atlantic Meridional Overturning Circulation (AMOC) variability in a coupled ocean–atmosphere GCM. *Adv. Atmos. Sci.*, **31**(2), 241–251, doi: 10.1007/s00376-013-3021-3.

## 1. Introduction

The temperature difference between low and high latitudes is regulated by solar heating and poleward heat transport, with the latter being almost equally important within the atmosphere and global oceans at mid-latitudes (Carissimo et al., 1985). In the Pacific, heat transport is poleward at mid-latitudes of 30°S and 30°N, with magnitudes of  $1 \times 10^{15}$ – $2 \times 10^{15}$  W (Hastenrath, 1982). In contrast, heat transport is northward at a magnitude of  $1 \times 10^{15}$  W from the South Atlantic to the North Atlantic (Hastenrath, 1982; Ganachaud and Wunsch, 2000). These meridional heat transports are largely associated with the Atlantic Meridional Overturning Circulation (AMOC). Therefore, changes in the AMOC can greatly impact on northward heat transport, which in turn affects European and global climate patterns (Clark et al., 2002; Pohlmann et al., 2006; Zhang and Delworth, 2007).

AMOC variability is largely controlled by surface heat flux, freshwater flux, and wind stresses in the Atlantic (Stommel, 1961; Rahmstorf, 1996; Kuhlbrodt et al., 2007; Huang et al., 2012, and references therein). Many studies based on observational analyses and ocean general circulation model

(OGCM) simulations suggest an important role of surface heat flux in AMOC variability (Eden and Willebrand, 2001; Häkkinen and Rhines, 2004; Böning et al., 2006; Huang et al., 2012). These studies found that changes in surface heat flux are directly driven by the North Atlantic Oscillation (NAO) (Hurrell, 1995; Hurrell et al., 2003). Further studies have shown that a higher NAO index can produce more Labrador Sea Water (LSW) by stronger convection (Bentsen et al., 2004; Kieke et al., 2007; Bower et al., 2009). In turn, LSW production can impact upon the strength of the subpolar gyre that is directly associated with AMOC strength (Eden and Willebrand, 2001; Böning et al., 2006; Balmaseda et al., 2007; Bower et al., 2009; Huang et al., 2012).

However, the conclusions associated with these studies are limited by sparse observations in space and time (Cunningham et al., 2007), which complicates studying the mechanisms controlling AMOC variability at decadal and longer timescales. Therefore, simulations with coupled models have become an important alternative for such studies; but even with this approach there are limitations, with inconsistencies found among key conclusions from coupled model simulations. For example, some studies have indicated that the NAO and its associated surface heat flux and wind stresses are critical to the changes of AMOC at various timescales (Dong and Sutton, 2005; Danabasoglu, 2008; Ortega et al., 2011),

\* Corresponding author: Boyin HUANG  
Email: boyin.huang@noaa.gov

while other studies have suggested that salinity could play a more important role in AMOC variability (Frankignoul et al., 2009; Msadek and Frankignoul, 2009; Zhang et al., 2009).

This paper was motivated by our previous study based on a 30-yr ocean reanalysis from 1979 to 2008 (Huang et al., 2012). We previously found that changes in AMOC are directly associated with subsurface temperature anomalies, which can be traced back further to changes in surface heat flux. However, it was not clear how AMOC variability is coupled with surface heat flux. Here, we focus on how AMOC variability interacts with surface forcing using a 2000-yr simulation of a coupled atmosphere–ocean general circulation model, as well as whether the conclusions based on ocean reanalysis are valid in a coupled ocean–atmosphere system. We begin by briefly describing the model (section 2) and simulated AMOC variability (section 3). Then, we present how AMOC is coupled with SST and surface heat flux (section 4) and subsurface temperature (section 5); how it is forced by surface heat flux (section 6); and how it is associated with subsurface temperature, salinity and density (section 7). Finally, a summary and discussion are provided in section 8.

## 2. Fast Ocean–Atmosphere Model

We used the Fast Ocean–Atmosphere Model (FOAM) (Jacob, 1997), which includes a low-resolution atmosphere model of approximately  $7.5^\circ \times 4^\circ$  in longitude and latitude of R15 with 18 levels, ocean model of  $2.8^\circ \times 1.4^\circ$  in longitude and latitude with 32 levels, and a land surface model of  $2.8^\circ \times 1.4^\circ$  in longitude and latitude with four layers. The capabilities of FOAM in simulating climate and climate change were reviewed by Liu et al. (2003). In particular, the capabilities of FOAM in simulating decadal and multi-decadal variabilities in the North Pacific and North Atlantic have been demonstrated in extensive studies by Wu and Liu (2003, 2005).

The atmospheric model is based on Community Climate Model 3 (CCM3) (Buja and Craig, 2002) of the National Center for Atmospheric Research (NCAR). The numerical scheme of the ocean model follows the Modular Ocean Model (MOM version 1) of the Geophysical Fluid Dynamics Laboratory (GFDL). The ocean model uses a finite-difference of A-grid and a free surface in the  $z$ -coordinate, and is parallel in its calculations. The horizontal mixing coefficient is constant, while the vertical mixing is dependent on the Richardson number. The land surface model explains five main vegetation types and is principally the same as CCM3, except with the following modifications: a simple bucket model is replaced by a 15-cm deep bucket model; evaporation is set to be proportional to the water depth within the bucket; the prescribed snow coverage is replaced by a simple prognostic scheme; the bucket overflow is taken as river runoff and routed to a parallel river transport model. The FOAM sea ice component includes thermodynamics of the NCAR Climate System Model without sea ice dynamics. The time steps are

0.5 h for the atmospheric, land surface and sea ice models, and 6 h for the ocean model. The coupler calculates the fluxes between the atmosphere and oceans in the overlap grids once every 6 h, which are used by the atmosphere or ocean model without flux correction. The model was spun up for 1000 yr with a constant  $\text{CO}_2$  concentration of 335 ppmv and reached a quasi-equilibrium state. The model was then run for an additional 2000 yr (year 1–2000, hereafter) with the same  $\text{CO}_2$  concentration, which is used in our analysis. The model outputs monthly data that are processed into an annual average. The annual anomalies are the deviation from the climatology of year 1–2000.

## 3. AMOC variability

We used Empirical Orthogonal Functions (EOFs) and their associated Principle Components (PCs) to quantify the dominant modes of the spatial and temporal variability of AMOC, as in other studies (e.g., Bentsen et al., 2004; Huang et al., 2012). To fairly account for the AMOC variances at different model levels, the AMOC stream function at a non-uniform model depth was interpolated to a uniform interval of 100 m. The EOFs of AMOC were then assessed in a domain of  $30^\circ\text{S}$  and  $65^\circ\text{N}$  in the upper 4000 m. Figure 1a shows the first EOF (EOF1) of AMOC, which explains 44% of the total variance with a maximum variability of 3.5 Sv ( $1 \text{ Sv} = 10^6 \text{ m}^3 \text{ s}^{-1}$ ) near  $52^\circ\text{N}$  and 1750 m depth. The magnitude of AMOC variability is comparable with the simulation of Bentsen et al. (2004) and the reanalysis of Huang et al. (2012), but stronger than the simulation of Medhaug et al. (2011). The location of the maximum variability is very close to that of Huang et al. (2012), but approximately  $5^\circ$ – $10^\circ$  northward than those in Bentsen et al. (2004) and Medhaug et al. (2011), which may indicate that the location of deep convection is relatively more northward in FOAM.

The temporal variability of simulated AMOC EOF1 was quantified by the first Principal Component (PC1) (Fig. 1b). The spectrum analysis shows that the PC1 of AMOC exhibits a wide range of dominant periods at 15–35, 40, 50 and 60 yr (Fig. 1c), as were reported in previous studies (20–80 yr) (Dong and Sutton, 2005; Danabasoglu, 2008; Medhaug et al., 2011). The temporal variability of AMOC can also be quantified by the maximum AMOC near  $55^\circ\text{N}$ , which is highly (0.79) correlated with AMOC PC1 (Fig. 1b). The maximum AMOC is defined as the maximum streamfunction in the vertical direction where the climatological AMOC reaches a maximum near  $55^\circ\text{N}$ . Note that the cross correlation coefficient is considered to be significant at the 95% level if it is larger than 0.25 (0.16), assuming an independent sampling number larger than 62 (145). The sampling number was estimated using a cut-off auto correlation coefficient of 0.1 (0.3) in the AMOC time series of 2000 yr after a 7-yr running average (von Storch and Zwiers, 2001). EOFs, PCs and correlation coefficients were calculated using data of year 1–2000, although time series of PCs were mostly plotted for year 1–1000.

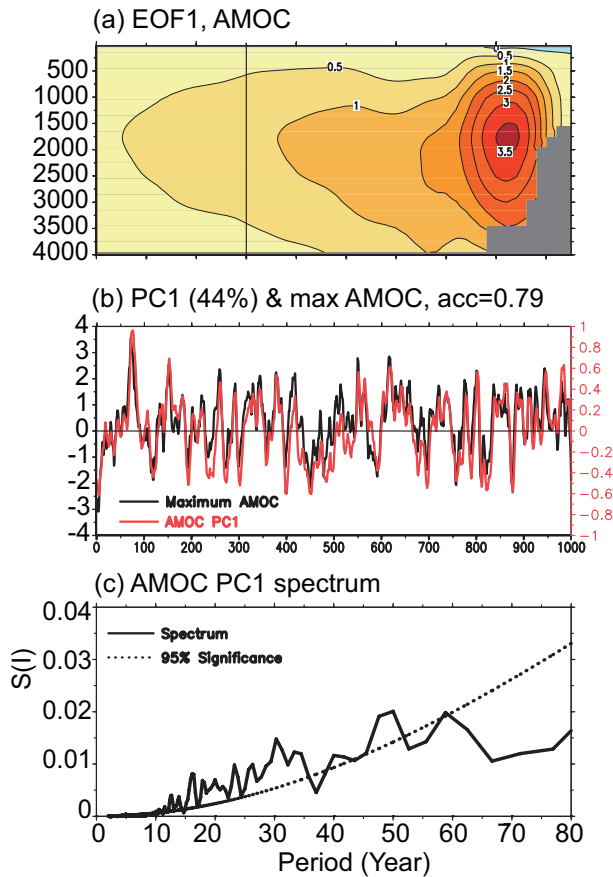


**Fig. 1.** (a) EOF1 of AMOC stream function with contour interval of 0.5 Sv; (b) PC1 of AMOC (right axis) and maximum AMOC anomaly (left axis; Sv); (c) spectrum density and its 95% confidence level of AMOC PC1 as a function of period. The EOF1 contains 44% of total variance in (a). A 7-yr running mean is applied in (b).

#### 4. AMOC coupled with SST and surface heat flux

To assess the relationship between AMOC and surface forcing, we start with linear regressions of SST, sea surface salinity (SSS) and surface density to AMOC. The analysis shows that, for a given one Sv increase in AMOC, SST increases by 0.06°C in the northeastern North Atlantic and between 25°N and 45°N, and decreases by 0.02°C in the Labrador Sea (Fig. 2a), which is consistent with Delworth et al. (1993) but slightly different from Timmermann et al. (1998). SSS increases by 0.03 psu in the northern North Atlantic (Fig. 2b). Therefore, density increases by 0.015 kg m<sup>-3</sup> in the northern North Atlantic north of 50°N (Fig. 2c), which is dominated by increased salinity, shown in Fig. 2b. The density change associated with salinity may indicate a very important role of salinity in AMOC variability (Danabasoglu, 2008; Frankignoul et al., 2009; Msadek and Frankignoul, 2009) and will be discussed further in section 5.

To help understand the interactions between AMOC and atmospheric forcing, we analyzed the EOF1s and their

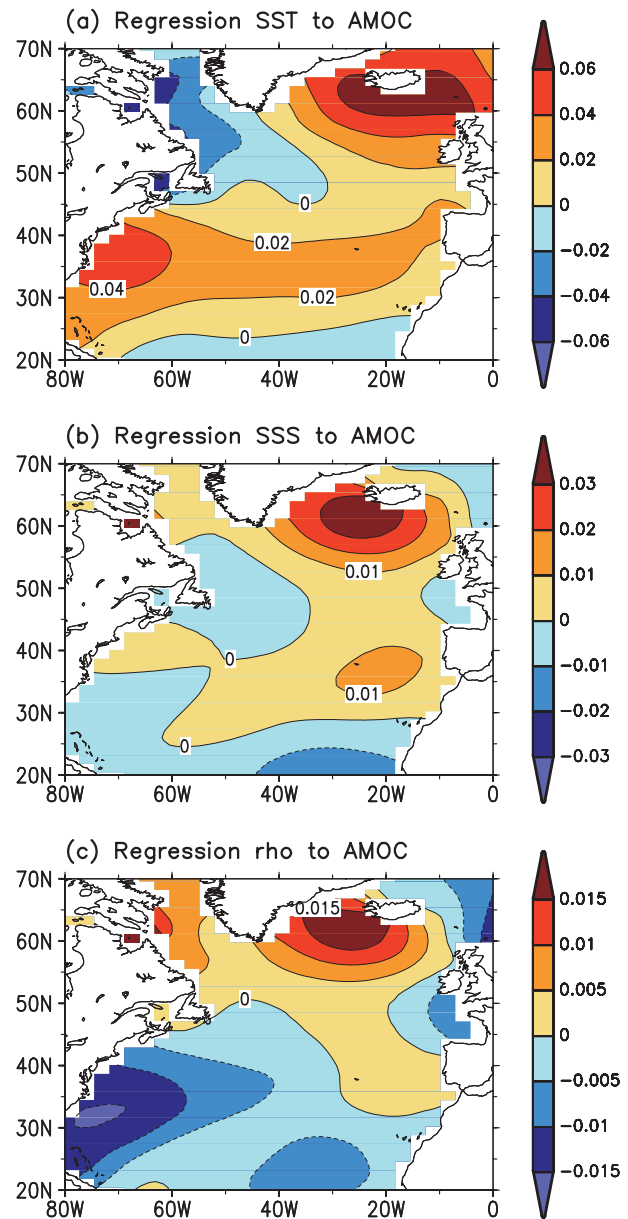


**Fig. 2.** Linear regressions of (a) SST; (b) SSS; and (c) density to AMOC. Contour intervals are 0.02°C, 0.01 psu, and 0.005 kg m<sup>-3</sup> per Sv in (a), (b) and (c), respectively.

associated PC1s of SST and surface heat flux within a domain of 20°–70°N and 0–80°W, which explain close to 30% of the total variance. The surface heat flux is defined as positive when the ocean absorbs heat. Our analysis shows that, when AMOC increases, the SST increases by 0.8°C in the northeastern North Atlantic, which stretches southeastward to the subtropical western North Atlantic (Fig. 3a). Figure 3d shows the PC1s of SST and AMOC filtered by a 10-yr running mean. Their correlation coefficient is 0.48 with a 0-yr lag, which suggests that the increase in SST is associated with northward heat transport by AMOC.

Similar to the spatial pattern of SST, the surface heat flux increases by 10 W m<sup>-2</sup> in the northeastern North Atlantic

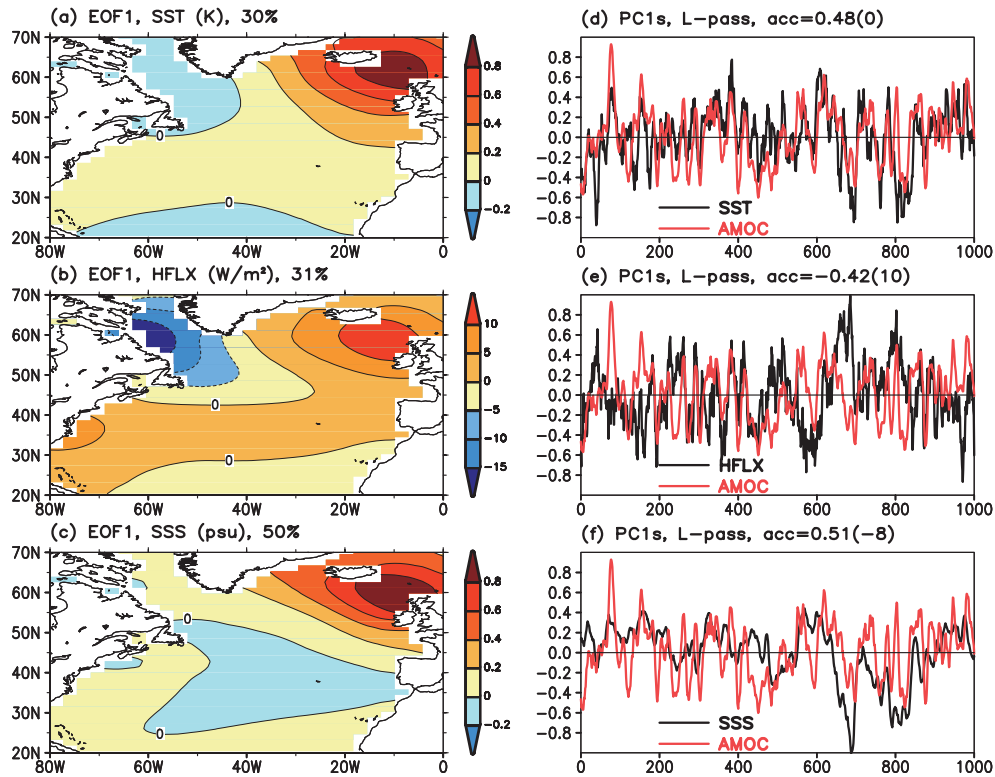


**Fig. 3.** EOF1s of (a) SST; (b) surface heat flux (positive values indicate heating of the ocean); and (c) SSS. Panels (d)–(f) show the low-pass ( $\geq 10$  yr) filtered PC1s in (a)–(c), respectively. EOF1 explains 30%, 31% and 50% of the total variance in (a), (b) and (c), respectively. Contour intervals are  $0.2^{\circ}\text{C}$ ,  $5 \text{ W m}^{-2}$  and  $0.2 \text{ psu}$  in (a), (b) and (c), respectively.

and stretches southeastward (Fig. 3b). Further analysis indicates that the PC1 of surface heat flux is negatively correlated ( $-0.41$ ) with the PC1 of SST and surface heat flux leads SST by approximately 10 yr. Furthermore, the PC1 of surface heat flux is also negatively correlated ( $-0.42$ ) with the PC1 of AMOC and surface heat flux leads AMOC by 10 yr (Fig. 3e). These results indicate that the changes in surface heat flux are forced by SST. The changes in SST are likely driven by meridional heat transport associated with AMOC variability at decadal and longer timescales, and the AMOC variability is coupled with SST and surface heat flux. These aspects will be discussed further in section 5.

Analyses suggest that the negative correlation between the PC1s of surface heat flux and AMOC at decadal and longer timescales results from the integrated heating ( $1.5 \times 10^{13} \text{ W}$ ) over the North Atlantic between  $20^{\circ}\text{N}$  and  $70^{\circ}\text{N}$  (Fig. 3b), since the heat added to the surface water is advected to the downwelling region of the AMOC at decadal and longer timescales (Huang et al., 2003; Bugnion et al., 2006). For example, an integrated heating to the North Atlantic slows down the AMOC so that the northward heat transport and SST decrease in the North Atlantic. The decrease in SST may further increase the heating to the ocean due to reduced latent and sensible heat fluxes and thus form a positive feedback loop, as indicated schematically in Fig. 4 (black arrows).

However, it should be noted that the anomaly of surface

heat flux is strong in the Labrador Sea and surrounding regions (Fig. 3b) where the SST anomaly is very weak. The reason for a weak SST anomaly may be that the mean mixed layer depth (MLD) is deep (close to 2500 m in winter; not shown in the figure) in the Labrador Sea and surrounding regions. Therefore, the surface heat flux can effectively penetrate into the deeper ocean by convection and/or the downwelling branch of mean AMOC such that SST is not greatly affected by surface heat flux (Huang et al., 2003). In contrast, the mean MLD is much shallower in the northeastern North Atlantic, which enhances the variability of SST by the surface heat flux.

## 5. AMOC coupled with subsurface temperature

However, the changes in AMOC are regulated by subsurface temperature. For example, a weakened AMOC decreases the subsurface temperature via weaker northward heat transport. The decrease in subsurface temperature acts as a negative feedback to prevent the AMOC from weakening further by enhancing the density in the higher latitudes (Fig 4; blue arrows). The change of subsurface temperature is demonstrated by the second EOF (EOF2) of the basin-averaged subsurface temperature (Fig. 5a), which explains 12% of the total variance within  $20^{\circ}$ – $70^{\circ}\text{N}$  and 0–4000 m. The EOF1 of subsurface temperature appears to be forced

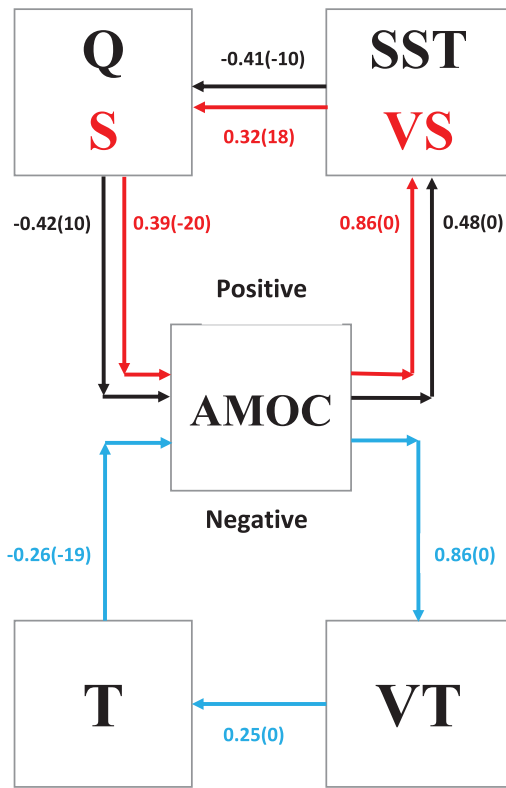


**Fig. 4.** Schematic diagram depicting the coupled mode of the ocean and atmosphere associated with AMOC variability. The loops of Q–AMOC–SST–Q (black) and S–AMOC–VS–S (red) represent positive feedback. The loop AMOC–VT–T–AMOC (blue) represents negative feedback. The numbers represent the correlation coefficients and phase leads. For example, the correlation coefficient between Q and AMOC is  $-0.42$ , and Q leads AMOC by 10 yr.

directly by surface heat flux, which will be discussed in section 6. Figure 5a shows temperature anomalies from  $0.1^{\circ}\text{C}$  to  $0.3^{\circ}\text{C}$  in the upper North Atlantic above 1000 m, and from  $-0.1^{\circ}\text{C}$  to  $-0.3^{\circ}\text{C}$  in the lower North Atlantic between 1000 and 2500 m. Further analysis shows that these subsurface temperature anomalies are associated with changes in AMOC. The second PC (PC2) of the subsurface temperature is correlated (0.23) with the PC1 of AMOC with a near 0-yr lag (Fig. 5b), which represents an instantaneous response of subsurface temperature to an increased AMOC. However, as the upper ocean temperature increases, the density decreases, meaning the increased AMOC is eventually suppressed after 19 yr, which represents a delayed response of surface temperature and works as a negative feedback to AMOC variability (Fig. 4; blue arrows). The lagged (19 yr) correlation coefficient is  $-0.26$ .

An evaluation of northward heat transport (not shown), defined as the product of meridional current and temperature (VT) in the North Atlantic, confirms that AMOC is correlated (0.86; 0-yr lag) with meridional heat transport (Fig. 4), which is further correlated (0.25; 0-yr lag) with basin-averaged temperature. Therefore, the relationships of AMOC with surface heat flux, SST, and subsurface temperature at decadal and

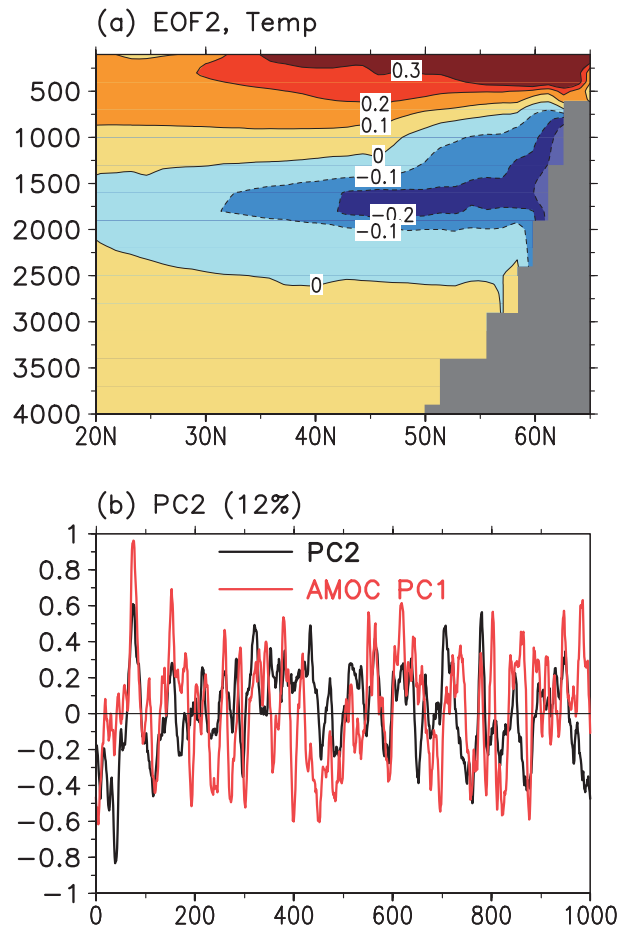


**Fig. 5.** (a) EOF2 of temperature and (b) PC2 of temperature along with the PC1 of AMOC. Contour interval is  $0.1^{\circ}\text{C}$  in (a). The EOF2 explains 12% of the total variance. A 7-yr running mean is applied in (b).

longer timescales represents a coupled mode of the ocean and atmosphere.

It is important to note that the role of salinity is also critical in AMOC variability. For example, as the AMOC slows down, northward salt transport weakens, and therefore SSS decreases in the northeastern North Atlantic (Figs. 3c and 2b; note that positive SSS in the figures is relative to a strengthened AMOC). The lower SSS further weakens the AMOC and therefore intensifies the positive feedback loop at decadal and longer timescales (Fig. 4; red arrows). This is indicated by a positive (0.51) correlation between SSS and AMOC with a lag of SSS by approximately 8 yr (Fig. 3f). The analysis shows that the PC2 of subsurface salinity lags the PC1 of AMOC by approximately 20 yr with a correlation coefficient of 0.39, although the EOF2 of subsurface salinity appears to be shallow (not shown). The northward salt transport (VS), which is defined as the production of meridional current and salinity (VS) in the latitude–depth plane, leads salinity variability by 18 yr with a correlation coefficient of 0.32, and is well correlated (0.86) with AMOC at a 0-yr lag. Therefore, we believe that the salinity variabilities near the surface are driven by AMOC, which will be discussed in section 6.

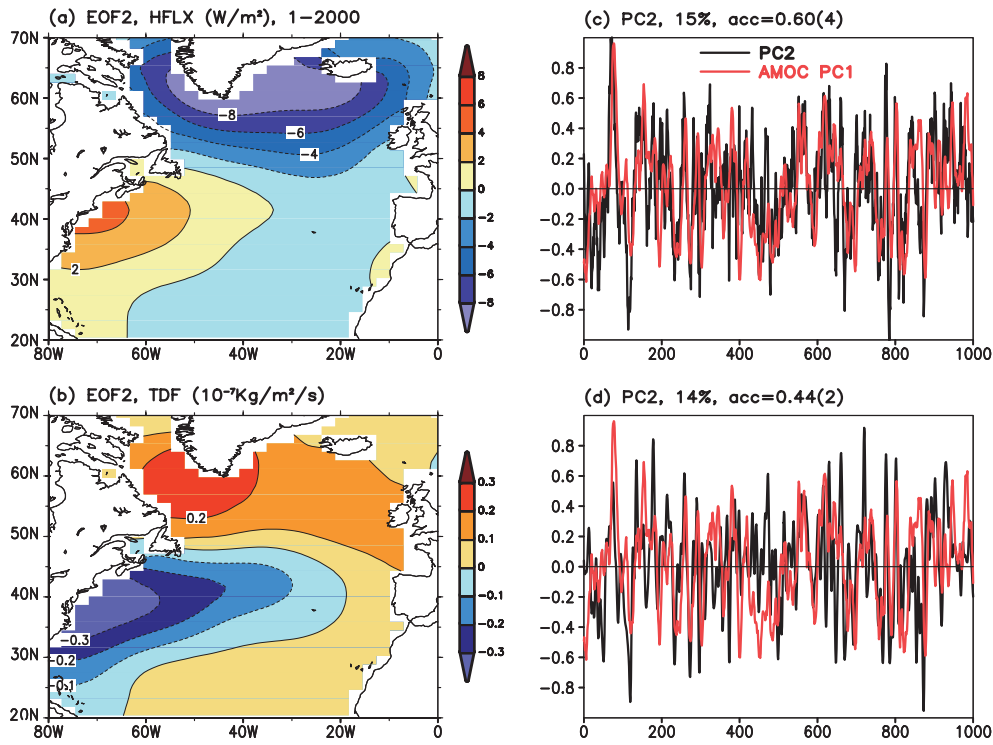


**Fig. 6.** EOF2s of (a) surface heat flux and (b) thermal density flux; and PC2 of (c) surface heat flux and (d) thermal density flux. The EOF2 contains 15% and 14% of the total variance in (a) and (b), respectively. The contour interval is  $2 \text{ W m}^{-2}$  and  $0.1 \times 10^{-7} \text{ kg m}^{-2} \text{ s}^{-1}$  in (a) and (b), respectively. Positive values in (a) and (b) indicate a heating and densifying of the ocean, respectively. A 7-yr running mean is applied in (c) and (d).

## 6. AMOC forced by surface heat flux

In addition to the coupled mode of surface heat flux, Figs. 6a and b show the EOF2s of surface heat and associated thermal density fluxes (Schmitt et al., 1989; Shin et al., 2003) within a domain of  $20^{\circ}$ – $70^{\circ}\text{N}$  and  $0^{\circ}$ – $80^{\circ}\text{W}$ . The EOF2s explain approximately 14% of the total variance of surface heat and thermal density fluxes. It is clear that the EOF2 patterns of surface heat and thermal density fluxes are largely consistent. For example, a cooling of  $6 \text{ W m}^{-2}$  north of  $45^{\circ}\text{N}$  corresponds with an increased thermal density flux of  $0.2 \times 10^{-7} \text{ kg m}^{-2} \text{ s}^{-1}$ ; and a warming of  $4 \text{ W m}^{-2}$  in the western North Atlantic between  $30^{\circ}\text{N}$  and  $45^{\circ}\text{N}$  corresponds with a decreased thermal density flux of  $0.3 \times 10^{-7} \text{ kg m}^{-2} \text{ s}^{-1}$ . An important feature of Fig. 6 is that maximum correlation coefficients are found between the PC1 of AMOC and the PC2 of heat flux (0.60; Fig. 6c), and also between the PC1 of AMOC and PC2 of thermal density flux (0.44; Fig. 6d). The PC2s of surface heat flux and associated thermal density flux lead the PC1 of AMOC by approximately 4 and 2 yr, respectively, as indicated in other studies (3–6 yr) (Medhaug et al., 2011; Ortega et al., 2011; Huang et al., 2012). Therefore, we argue that the EOF2s of surface heat flux and associated thermal density flux are a forcing mode of the atmosphere to AMOC variability at the interannual timescale, as displayed schematically in Fig. 7.

In contrast to the strong impact of surface heat flux on AMOC, the impact from surface freshwater flux (precipita-

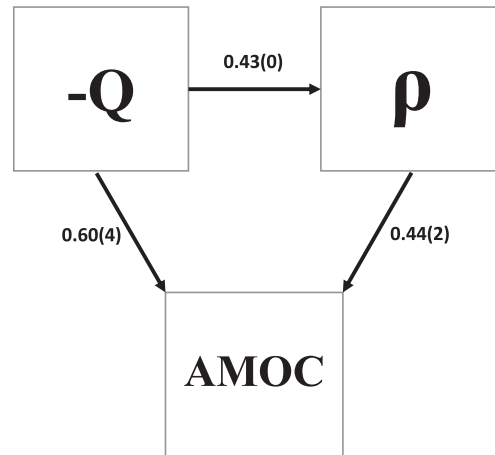


**Fig. 7.** Schematic diagram depicting the forcing mode of the surface heat flux associated with AMOC variability. Decreased surface heat flux ( $-Q$ ) in the higher latitudes enhances density ( $\rho$ ) and therefore its meridional gradient, which in turn strengthens the AMOC. The numbers represent correlation coefficients and phase leads (yr).

tion, river runoff, sea-ice melting, and evaporation;  $P + R + M - E$ ) is much weaker. The thermal density flux due to surface heat flux (Fig. 8a) is much larger than the haline density flux due to surface freshwater flux (Fig. 8b). Therefore, AMOC variability is dominated by the surface heat flux of

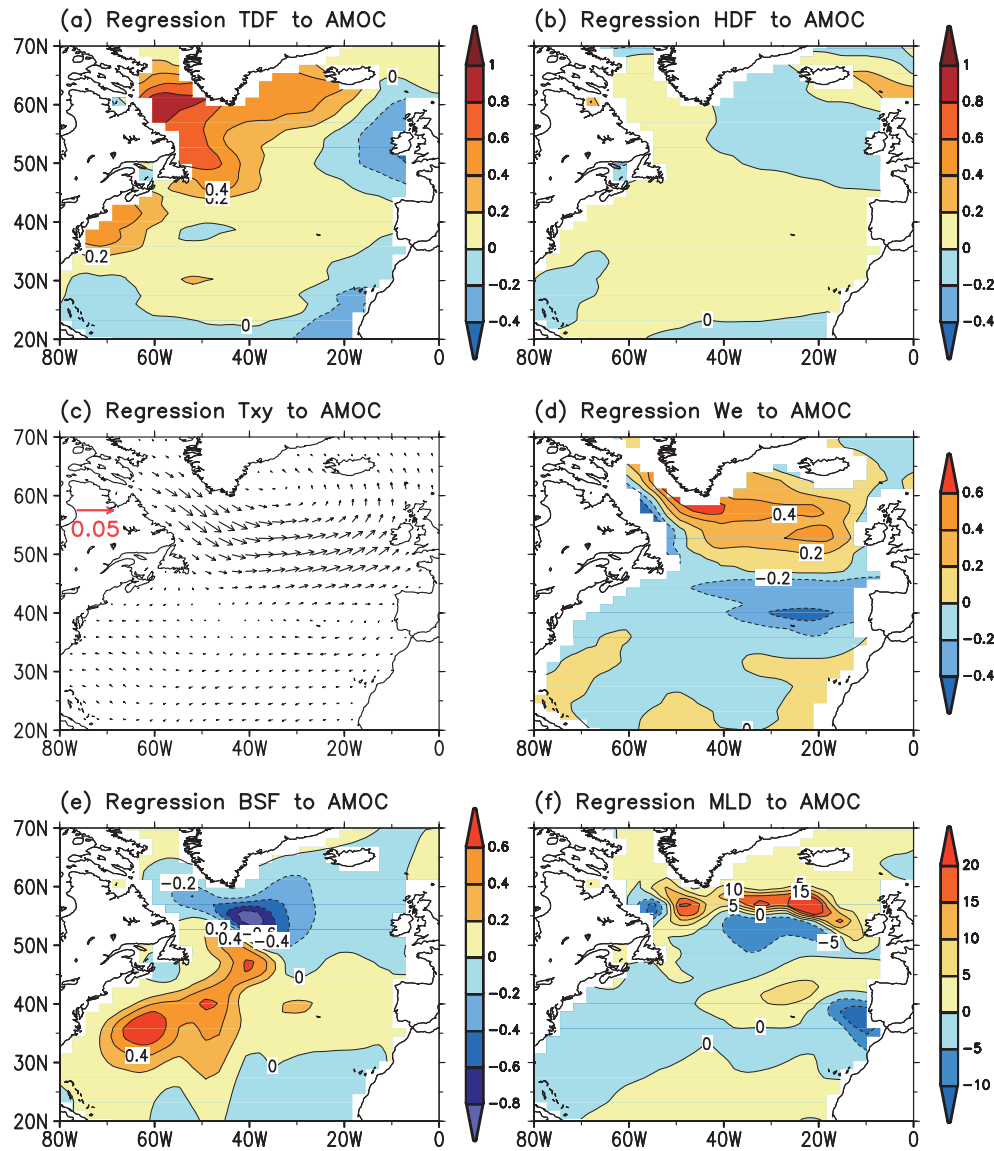


**Fig. 8.** Linear regressions of (a) thermal density flux; (b) haline density flux; (c) wind stresses; (d) Ekman pumping; (e) barotropic streamfunction; and (f) wintertime MLD to AMOC PC1. Contour units are  $10^{-7} \text{ Kg m}^{-2} \text{ s}^{-1}$  in (a) and (b),  $\text{dyn cm}^{-2}$  in (c),  $10^{-5} \text{ cm s}^{-1}$  in (d), Sv in (e) and m in (f) for 1Sv increase in AMOC.

the forcing mode, as suggested in other studies (Eden and Willebrand, 2001; Häkkinen and Rhines, 2004; Böning et al., 2006; Ortega et al., 2011; Medhaug et al., 2011; Huang et al., 2012).

Surface wind stresses (Fig. 8c) may play an important role in AMOC variability. Corresponding to a 1 Sv increase in AMOC, a strong ( $0.02 \text{ dyn cm}^{-2}$ ) northwesterly is found over the Labrador Sea, as well as a westerly over the central North Atlantic and a southeasterly over the eastern North Atlantic between  $45^{\circ}\text{N}$  and  $65^{\circ}\text{N}$ . These cyclonic wind stresses form the Ekman upwelling ( $0.4 \times 10^{-5} \text{ cm s}^{-1}$ ) between  $45^{\circ}\text{N}$  and  $65^{\circ}\text{N}$  and downwelling ( $-0.2 \times 10^{-5} \text{ cm s}^{-1}$ ) between  $30^{\circ}\text{N}$  and  $45^{\circ}\text{N}$  (Fig. 8d). The downwelling south of  $45^{\circ}\text{N}$  tends to enhance the AMOC (Dong and Sutton, 2005; Köhl, 2005; Huang et al., 2012), while the upwelling north of

$45^{\circ}\text{N}$  tends to suppress the AMOC from strengthening.

Associated with surface Ekman pumping, both subpolar and subtropical gyres enhance by 0.6 Sv (Fig. 8e). The relationship between AMOC and subpolar gyre is also suggested in ocean reanalysis (Balmaseda et al., 2007; Huang et al., 2012). According to the study by Böning et al. (2006), the strengthening of the subpolar gyre is associated with a stronger transport of the Deep Labrador Current (DLC), and therefore a stronger AMOC. The study by Kieke et al. (2007) further suggested that DLC production is associated with convection activities and deep water formation.

To evaluate the role of convection activity in AMOC variability, we calculated the maximum linear regression of MLD of boreal winter (January–March) to AMOC variability (Fig. 8f). The MLD is quantified by a monthly temperature dif-

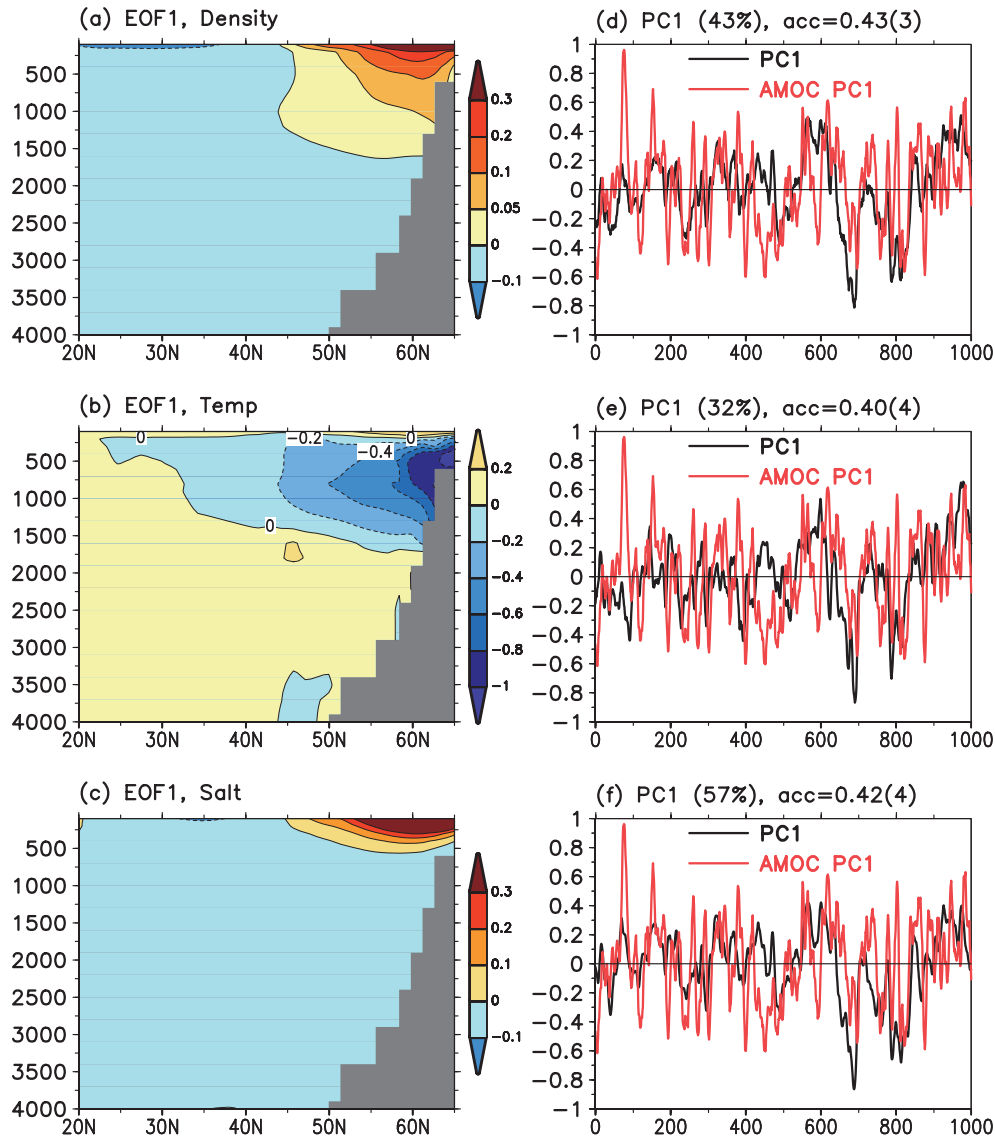


**Fig. 9.** EOF1s of (a) density; (b) temperature; and (c) salinity; as well as the PC1 of (d) density; (e) temperature; and (f) salinity, along with the PC1 of AMOC. The EOF1 explains 43%, 32% and 57% of the total variance in (a), (b) and (c), respectively. Contour units are  $\text{kg m}^{-3}$ ,  $^{\circ}\text{C}$  and psu in (a), (b) and (c), respectively. A 7-yr running mean is applied in (d)–(f).

ference of  $0.3^{\circ}\text{C}$  between the surface and the bottom of the mixed layer. It is found that MLD increases at approximately 20 m per 1-Sv increase in AMOC within a narrow latitudinal belt near  $55^{\circ}\text{N}$ , which leads AMOC by approximately 2 yr. Other studies, however, have indicated that MLD changes are confined to within the Labrador and Irminger Seas and lead AMOC by approximately 3–4 yr (Timmermann et al., 1998; Dong and Sutton, 2005; Huang et al., 2012).

## 7. AMOC forced by subsurface temperature, salinity and density

The subsurface temperature, salinity and density vary when they are forced by surface heat and freshwater fluxes,

which is demonstrated by their EOF1s and associated PC1s within a domain of  $20^{\circ}$ – $70^{\circ}\text{N}$  and 0–4000 m in Fig. 9. The EOF1s explain 32%–57% of the total variance. Our analysis suggests a close relationship of AMOC with density, temperature and salinity. For example, the density increases by  $0.1$ – $0.3 \text{ kg m}^{-3}$  north of  $45^{\circ}\text{N}$  above 1500 m (Fig. 9a), which can directly result in an increase in AMOC. The density increase is largely attributed to the  $0.2^{\circ}\text{C}$ – $0.8^{\circ}\text{C}$  cooling in temperature north of  $45^{\circ}\text{N}$  between 250 m and 1500 m (Fig. 9b), and partly attributed to the 0.3-psu increase in salinity north of  $45^{\circ}\text{N}$  above 500 m (Fig. 9c). The comparisons show that the PC1 of AMOC lags (by 3–4 yr) and is correlated (approximately 0.4) with the PC1s of density, temperature and salinity. Therefore, we argue that these EOF1s represent the variability of density, temperature and salinity associated with the

forcing mode of the surface heat flux, and contribute directly to AMOC variability.

Clearly, the density anomaly associated with AMOC variability can be largely attributed to the salinity anomaly north of 45°N above 500 m. However, the salinity anomaly associated with AMOC variability may not be directly forced by surface freshwater flux. The reason is that the salinity anomaly contributing to the density anomaly is not forced by anomalous surface freshwater flux associated with AMOC variability (Fig. 8b). Comparisons indicate that the patterns of the EOF1s of density and temperature north of 45°N are very similar to those in ocean reanalysis (Huang et al., 2012). The difference is that the anomalies of density and temperature south of 45°N are very weak in this analysis, while they are of the same magnitude, but with opposite signs to those north of 45°N in the ocean reanalysis. The PC1s of density and temperature lead the PC1 of AMOC by 3–4 yr in this analysis, while they lead by 1–2 yr in the ocean reanalysis. The simulation reported by Msadek and Frankignoul (2009) also indicated a 4-yr leading of density to AMOC variability.

It should be noted that the ocean temperature anomaly near the surface (100 m) is not negative in the higher latitudes (Fig. 9b), as it should intuitively be attributed to surface cooling. The reason for this weak positive temperature anomaly may be associated with an increase in salinity near the surface (Fig. 9c), which triggers the convection and warms the near-surface water by relatively warmer subsurface water. It should also be noted that the phase relationships among the surface forcing, subsurface temperature and density, as well as AMOC, are not perfect. For example, the PC2 of surface heat flux (Fig. 6d) and PC1 of subsurface temperature (Fig. 9e) lead the PC1 of AMOC by approximately 4 yr. The PC2s of surface thermal density flux (Fig. 6d) and subsurface density (Fig. 9d) lead the PC1 of AMOC by 2–3 yr. These differences may indicate a complicated nature of AMOC variability. However, further analysis indicates that the PC2s of surface heat and thermal density fluxes lead the PC1s of subsurface temperature and density by 1–2 yr. Therefore, it is clear that there exists a forcing mode of surface heat flux driving the variability of subsurface temperature, meridional gradient of density, and AMOC.

## 8. Summary and discussion

The mechanisms of AMOC variability were studied using a 2000-yr coupled simulation of FOAM. It was found that AMOC variability is associated with a coupled mode between surface heat flux and SST, and is also associated with a forcing mode of surface heat flux.

The coupled mode of surface heat flux and SST interacts with AMOC at decadal timescales. Surface heat flux leads AMOC and SST by approximately 10 yr. It is suggested that the positive feedback induced by the coupling among AMOC, SST and surface heat flux is regulated by the northward heat transport as a negative feedback to AMOC variability. These conclusions are consistent with a recent study

by An et al. (2013).

The surface heat flux of the forcing mode leads AMOC by approximately 4 yr. The surface heat flux forcing directly impacts upon deep water formation, and therefore the meridional gradient of subsurface density and temperature across 50°N. The changes in density are largely attributed to the temperature change associated with anomalous surface heat flux in the North Atlantic. These conclusions are consistent with our previous study using 30-yr ocean reanalysis (Huang et al., 2012).

Additional analysis indicated that the changes in surface heat flux are largely associated with latent heat flux attributed to changes in wind speed, which is consistent with the studies of Häkkinen and Rhines (2004) and Huang et al. (2012). Furthermore, our study suggests that wind stresses may impact upon AMOC variability by direct surface Ekman pumping. The changes in wind stresses and speed are associated with the NAO, as indicated in earlier studies (Dong and Sutton, 2005; Danabasoglu, 2008; Ortega et al., 2011). The dynamic effect of wind in the subtropical gyre south of 45°N may be opposite to that in the subpolar gyre north of 45°N. Therefore, further study is required to assess their combined effect in both subtropical and subpolar gyres.

Near-surface salinity appears to be associated with meridional salt transport by AMOC variability, rather than with surface freshwater flux. However, we did not identify a clear pattern of subsurface salinity coupled with AMOC at decadal timescales, although we did identify a clear pattern of subsurface salinity associated with the atmospheric forcing mode at interannual timescales. However, studies by Frankignoul et al. (2009), Msadek and Frankignoul (2009) and Zhang et al. (2009) indicated that freshwater and its associated salinity changes play a critical role in AMOC variability. Further studies using different coupled models with higher resolutions are expected to clarify the role of salinity in AMOC variability and to validate whether our conclusions are model-dependent. In particular, sensitivity tests need to be carried out to verify the forcing mode and coupled mode associated with AMOC variability.

The simulations of FOAM indicate that AMOC variabilities may be associated with variabilities of Atlantic Multi-decadal Oscillation (AMO). Our analysis indicates that AMO is well described by the EOF2 of SST (not shown), with a correlation coefficient of 0.60 between AMO and the PC2 of SST. Furthermore, AMOC and AMO are correlated with a correlation coefficient of 0.37, and AMOC leads AMO by approximately 4 yr. The leading phase of AMOC to AMO suggests that AMOC forces AMO variabilities. This is different from a simultaneous correlation between AMO and AMOC in a coupled model simulation reported by Zhang (2008).

The reason for the relationship between AMOC and AMO (NAO) can be seen from their overlapped periods of dominant variabilities. Spectrum analysis showed that simulated AMO exhibits a major variability near 63 yr, which is close to the observed analysis of 60–70 yr (Knight et al., 2006) and one of the AMOC variabilities near 60 yr (Fig. 1b). Likewise, simulated NAO exhibits major variabilities

similar to the observed analysis at decadal timescales of 24 yr (Mann and Park, 1994; Hurrell and van Loon, 1997; Cook et al., 1998), which are within AMOC variabilities of 15–35 yr (Fig. 1c). These features suggest a linkage between AMO (NAO) and AMOC variabilities.

Finally, it is important to highlight that the mean AMOC (near 35 Sv) near 55°N in FOAM is strong if it is compared with other coupled models [from 14 to 32 Sv; Weaver et al. (2012)]. The strong AMOC in FOAM may result from coarse model resolutions and/or stronger local convections extending from the Labrador Sea to the interior northern North Atlantic (Fig. 8f), while observations indicate that the convections are confined mostly to within Labrador Sea. The stronger convection may be associated with the simple parameterization of vertical mixing—most state-of-the-art models use Gent and McWilliams (1990) isopycnal mixing. In the lower latitudes south of 45°N, the AMOC strength (near 15 Sv) and structure are comparable with observations (Cunningham et al., 2007) and modern data assimilation systems (Tony Lee, personal communication).

**Acknowledgements.** The authors wish to thank the two anonymous reviewers, whose constructive comments greatly improved the manuscript. HY and JZ were supported by the National Natural Science Foundation of China (No. 41176002).

## REFERENCES

- An, S. I., H. Kim, and B. M. Kim, 2013: Impact of freshwater discharge from the Greenland ice sheet on North Atlantic climate variability. *Theor. Appl. Climatol.*, doi: 10.1007/s00704-012-0699-6.
- Balmaseda, M. A., and Coauthors, 2007: Historical reconstruction of the Atlantic meridional overturning circulation from the ECMWF operational ocean reanalysis. *Geophys. Res. Lett.*, **34**, L23515, doi: 10.1029/2007GL031645.
- Bentsen, M., and Coauthors, 2004: Simulated variability of the Atlantic meridional overturning circulation. *Climate Dyn.*, **22**, 701–720.
- Böning, C. W., and Coauthors, 2006: Decadal variability of subpolar gyre transport and its reverberation in the North Atlantic overturning. *Geophys. Res. Lett.*, **33**, L21S01, doi: 10.1029/2006GL026906.
- Bower, A. S., M. S. Lozier, S. F. Gary, and C. W. Böning, 2009: Interior pathways of the North Atlantic meridional overturning circulation. *Nature*, **459**, 243–248.
- Bugnion, V., C. Hill, and P. H. Stone, 2006: An adjoint analysis of the meridional overturning circulation in a hybrid coupled model. *J. Climate*, **19**, 3751–3767.
- Buja, L., and T. Craig, 2002: CCSM2.0.1 User's Guide. National Center for Atmospheric Research, 102 pp.
- Carissimo, B. C., A. H. Oort, and T. H. Vonder Haar, 1985: Estimating the meridional energy transports in the atmosphere and oceans. *J. Phys. Oceanogr.*, **15**, 82–91.
- Clark, P. U., N. G. Pisias, T. F. Stocker, and A. J. Weaver, 2002: The role of the thermohaline circulation in abrupt climate change. *Nature*, **415**, 863–869.
- Cook, E. R., R. D. D'Arrigo, and K. R. Briffa, 1998: A reconstruction of the North Atlantic Oscillation using tree-ring chronologies from North America and Europe. *The Holocene*, **8**, 9–17.
- Cunningham, S. A., and Coauthors, 2007: Temporal variability of the Atlantic meridional overturning circulation at 26.5°N. *Science*, **317**, 935–938, doi: 10.1126/science.1141304.
- Danabasoglu, G., 2008: On multidecadal variability of the Atlantic meridional overturning circulation in the community climate system model version 3. *J. Climate*, **21**, 5524–5544.
- Delworth, T., S. Manabe, and R. J. Stouffer, 1993: Interdecadal variations of the thermohaline circulation in a coupled ocean-atmosphere model. *J. Climate*, **6**, 1993–2011.
- Dong, B., and R. T. Sutton, 2005: Mechanism of interdecadal thermohaline circulation variability in a coupled ocean-atmosphere GCM. *J. Climate*, **18**, 1117–1135.
- Eden, C., and J. Willebrand, 2001: Mechanism of interannual to decadal variability of the North Atlantic circulation. *J. Climate*, **14**, 2266–2280.
- Frankignoul, C., J. Deshayes, and R. Curry, 2009: The role of salinity in the decadal variability of the North Atlantic meridional overturning circulation. *Climate Dyn.*, doi: 10.1007/s00382-008-0523-2.
- Ganachaud, A., and C. Wunsch, 2000: Improved estimates of global ocean circulation, heat transport and mixing from hydrographic data. *Nature*, **408**, 453–457.
- Gent, P. R., and J. C. McWilliams, 1990: Isopycnal mixing in ocean circulation model. *J. Phys. Oceanogr.*, **20**, 150–155.
- Häkkinen, S., and P. B. Rhines, 2004: During the 1990s Decline of subpolar North Atlantic circulation. *Science*, **304**, doi: 10.1126/science.1094917.
- Hastenrath, S., 1982: On meridional heat transports in the world ocean. *J. Phys. Oceanogr.*, **12**, 922–927.
- Huang, B., P. H. Stone, S. P. Sokolov, and I. V. Kamenkovich, 2003: The deep-ocean heat uptake in transient climate change. *J. Climate*, **16**, 1352–1363.
- Huang, B., Y. Xue, A. Kumar, and D. W. Behringer, 2012: AMOC variations in 1979–2008 simulated by NCEP operational ocean data assimilation system. *Climate Dyn.*, **38**, doi: 10.1007/s00382-011-1035-z.
- Hurrell, J. W., 1995: Decadal trends in the North Atlantic oscillation regional temperatures and precipitation. *Science*, **269**, 676–679.
- Hurrell, J. W., and H. van Loon, 1997: Decadal variation in climate associated with the North Atlantic Oscillation. *Climatic Change*, **36**, 301–326.
- Hurrell, J. W., Y. Kushnir, G. Ottersen, and M. Visbeck, Eds., 2003: *The North Atlantic Oscillation Climate Significance and Environmental Impacts*. Geophysical Monograph Series, 134 pp.
- Jacob, R., 1997: Low frequency variability in a simulated atmosphere ocean system. Ph.D. thesis, University of Wisconsin-Madison, 177 pp.
- Kieke, D., M. Rhein, L. Stramma, W. M. Smethie, J. L. Bullister, and D. A. LeBel, 2007: Changes in the pool of Labrador Sea Water in the subpolar North Atlantic. *Geophys. Res. Lett.*, **34**, L06605, doi: 10.1029/2006GL028959.
- Knight, J. R., C. K. Folland, and A. A. Scaife, 2006: Climate impacts of the Atlantic Multidecadal Oscillation. *Geophys. Res. Lett.*, **33**, L17706, doi: 10.1029/2006GL026242.
- Köhl, A., 2005: Anomalies of meridional overturning: Mechanisms in the North Atlantic. *J. Phys. Oceanogr.*, **35**, 1455–1472.
- Kuhlbrodt, K., and Coauthors, 2007: On the driving processes

- of the Atlantic meridional overturning circulation. *Rev. Geophys.*, **45**, RG2001, doi: 10.1029/2004RG000166.
- Liu, Z., B. Otto-Bliesner, J. Kutzbach, L. Li, and C. Shields, 2003: Coupled Climate Simulation of the Evolution of Global Monsoons in the Holocene. *J. Climate*, **16**, 2472–2490.
- Mann, M. E., and J. Park, 1994: Global-scale modes of surface temperature variability on interannual to century timescales. *J. Geophys. Res.*, **99**, 25 819–25 833.
- Medhaug, I., H. R. Langehaug, T. Eldevik, T. Furevik T, and M. Bentsen, 2011: Mechanisms for decadal scale variability in a simulated Atlantic meridional overturning circulation. *Climate Dyn.*, doi: 10.1007/s00382-011-1124-z.
- Msadek, R., and C. Frankignoul, 2009: Atlantic multi-decadal oceanic variability and its influence on the atmosphere in a climate model. *Climate Dyn.*, **33**, 45–62, doi: 10.1007/s00382-008-0452-0.
- Ortega, P., E. Hawkins, and R. Sutton, 2011: Processes governing the predictability of the Atlantic meridional overturning circulation in a coupled GCM. *Climate Dyn.*, doi: 10.1007/s00382-011-1025-1.
- Pohlmann, H., F. Sienz, and M. Latif, 2006: Influence of the multi-decadal Atlantic meridional overturning circulation variability on European climate. *J. Climate*, **19**, 6062–6067.
- Rahmstorf, S., 1996: On the freshwater forcing and transport of the Atlantic thermohaline circulation. *Climate Dyn.*, **12**, 799–811.
- Schmitt, R. W., P. S. Bogden, and C. E. Dorman, 1989: Evaporation minus precipitation and density fluxes for the North Atlantic. *J. Phys. Oceanogr.*, **19**, 1208–1221.
- Shin, S.-I., Z. Liu, B. Otto, E. Brady, J. Kutzbach, and S. Harrison, 2003: A simulation of the Last Glacial Maximum climate using the NCAR CCSM. *Climate Dyn.*, **20**, 127–151, doi: 10.1007/s00382-002-0260-x.
- Stommel, H., 1961: Thermohaline convection with two stable regimes of flow. *Tellus*, **13B**, 224–230.
- Timmermann, A., M. Latif, R. Voss, and A. Grötzner, 1998: Northern Hemispheric interdecadal variability: A coupled air–sea mode. *J. Climate*, **11**, 1906–1931, doi: http://dx.doi.org/10.1175/1520-0442-11.8.1906.
- von Storch, H., and F. W. Zwiers, 2001: *Statistical Analysis in Climate Research*. Cambridge University Press, 484 pp.
- Weaver, A. J., and Coauthors, 2012: Stability of the Atlantic meridional overturning circulation: A model intercomparison. *Geophys. Res. Lett.*, **39**, L20709, doi: 10.1029/2012GL053763.
- Wu, L., and Z. Liu, 2003: Decadal variability in the North Pacific: The eastern North Pacific mode. *J. Climate*, **16**, 3111–3131.
- Wu, L., and Z. Liu, 2005: North Atlantic decadal variability: Air–sea coupling, oceanic memory, and potential Northern Hemisphere resonance. *J. Climate*, **18**, 331–349.
- Zhang, R., 2008: Coherent surface subsurface fingerprint of the Atlantic meridional overturning circulation. *Geophys. Res. Lett.*, **35**, L20705, doi: 10.1029/2008GL035463.
- Zhang, R., and T. L. Delworth, 2007: Impact of the Atlantic multi-decadal oscillation on North Pacific climate variability. *Geophys. Res. Lett.*, **34**, L23708, doi: 10.1029/2007GL031601.
- Zhang, S., A. Rosati, and M. J. Harrison, 2009: Detection of multidecadal oceanic variability by ocean data assimilation in the context of a “perfect” coupled model. *J. Geophys. Res.*, **114**, C12018, doi: 10.1029/2008JC005261.